CrystEngComm

Supramolecular assemblies of benzene-1,3,5-tricarboxylic acid and 3,5-substituted pyrazoles: Formation and structural Analysis

Journal:	*CrystEngComm*
Manuscript ID:	CE-ART-10-2014-002117.R1
Article Type:	Paper
Date Submitted by the Author:	19-Dec-2014
Complete List of Authors:	singh, udai; IIT Roorkee, Chemistry Tomar, Kapil; IIT Roorkee, Department of Chemistry Kashyap, Sujata; IIT Roorkee, Department of Chemistry

Supramolecular assemblies of benzene-1,3,5-tricarboxylic acid and 3,5-substituted pyrazoles: Formation and structural Analysis

Udai P. Singh*, Kapil Tomar, Sujata Kashyap

Department of Chemistry, Indian Institute of Technology Roorkee, Roorkee – 247 667, India, Correspondence e-mail: udaipfcy@iitr.ac.in

Abstract:

Different supramolecular assemblies of benzene-1,3,5-tricarboxylic acid (H_3BTC) with various substituted pyrazoles viz., 3,5-dimethylpyrazole ($Pz^{Me2}H$), 3,5-diisopropylpyrazole ($Pz^{iPr2}H$), 3-tert-butyl-5-isopropylpyrazole ($Pz^{tBu,iPr}H$), 3-phenyl-5-methylpyrazole ($Pz^{Ph,Me}H$), 3-cumenyl-5-methylpyrazole ($Pz^{Cum,Me}H$), 3,5-diphenylpyrazole ($Pz^{Ph2}H$) and 3,3′,5,5′-tetramethyl-4,4′-bipyrazole ($BPzH_2$) have been prepared. The present study demonstrates that the formation of hydrogen bond between protonated pyrazoles and anions provides a sufficient driving force for the directed assembly of varied supramolecular frameworks where H_3BTC nicely adjusts its cavity dimensions to accommodate the guest. Theoretical studies were performed to analyze the effect of different substituents on hydrogen-bond interaction energy of the resultant salts and co-crystals. Energies of the various synthons were also calculated to correlate their stability and occurrence with the change of substituent on pyrazole ring.

Key words: Benzene-1,3,5-tricarboxylic acid, Pyrazole, Crystal structure

Introduction

Crystal engineering has contributed a lot in understanding the process of supramolecular self-assembly via intermolecular interactions.[1,2] The long term objective of crystal engineering is to find out reliable and robust supramolecular synthons. For this purpose,

the ligands of different dimensions and functionalities have been synthesized by different workers. The pyrazoles, a very interesting class of heterocyclic compounds, have many biological and pharmaceutical properties.[3] The parent pyrazole forms linear chains through N–H···N hydrogen bonds, however an unexpected and remarkable changes in the crystal structure were reported when substituents are introduced at 3, 4 and 5 positions of the pyrazole ring, e.g., 3,5-dimethylpyrazole forms cyclic trimers, 3,5-ditertbutylpyrazole forms cyclic dimers, 3,5-diphenylpyrazole and 3,5-bis(trifluoromethyl)-1H-pyrazole forms cyclic tetramers (Scheme 1)[4-8]. Several other pyrazole derivatives with different substituents were studied by different workers for their solid state structures.[9-15]

Highly symmetric carboxylic acid like benzene-1,3,5-tricarboxylic acid (H_3BTC) has received considerable attention as building blocks in supramolecular synthesis because of its potential for the creation of exotic architectures through hydrogen bonding. H_3BTC formed extended networks with ligands like pyridyls, amines, phenols, amides and imidazoles.[16] The first approach to obtain non-interpenetration in H_3BTC was tried by Herbstein et al. by taking long chain alkanes as a guests.[17] Using the same strategy, pyrene inclusion complex of H_3BTC was synthesized that resemble the chicken-wire network.[18] H_3BTC also constructs honeycomb grids with 1,3,5-tri(4-pyridyl)-2,4,6-triazine, 4,4′-methylenebis(2,6-dimethylaniline) and ligands having NH_2 group.[19-21] "To the best of our knowledge, a very few literature is currently available for the salts or co-crystals of H_3BTC with the members of azoles family.[22-25]"

The present paper reports the synthesis, crystal structure, rational analysis, thermal stability and DFT calculations for the pyrazole based co-crystals or salts as we are of the

opinion that understanding of structural correlations in salts or co-crystal may facilitate the design of new pyrazole based materials.

Results and discussion

The reaction of benzene-1,3,5-tricarboxylic acid (H_3BTC) with various substituted pyrazoles, viz., 3,5-dimethylpyrazole ($Pz^{Me2}H$), 3,5-diisopropylpyrazole ($Pz^{iPr2}H$), 3-tert-butyl-5-isopropylpyrazole ($Pz^{tBu,iPr}H$), 3-phenyl-5-methylpyrazole ($Pz^{Ph,Me}H$), 3-cumenyl-5-methylpyrazole ($Pz^{Cum,Me}H$), 3,5-diphenylpyrazole ($Pz^{Ph2}H$) and 3,3′,5,5′-tetramethyl-4,4′-bipyrazole ($BPzH_2$) yielded co-crystals or salts namely, $[H_2BTC^-.Pz^{Me2}H_2^+]$ **(1)**, $[H_3BTC.H_2BTC^-.Pz^{iPr2}H_2^+.H_2O]$ **(2)**, $[H_3BTC.H_2BTC^-.Pz^{tBu,iPr}H_2^+.H_2O]$ **(3)**, $[H_3BTC.Pz^{Ph,Me}H]$ **(4)**, $[H_3BTC.H_2BTC^-.Pz^{Cum,Me}H_2^+]$ **(5)**, $[H_2BTC^-.Pz^{Ph2}H_2^+.Pz^{Ph2}H.CH_3OH]$ **(6)** and $[2H_2BTC^-.BPzH_4^{2+}.CH_3OH]$ **(7)** (scheme 2). The different formulations were confirmed by elemental analysis, IR and X-ray crystallography. In case of salts (**1**-**3** & **5**-**7**) the proton has been transferred from carboxylic acid to the nitrogen of the pyrazole bearing lone pair of electron. The formation of these salts and co-crystals were also supported by C–O and C=O bond distances in their crystal structure.[26] The stretching frequencies of carbonyl group in the above compounds lies below or around 1706 cm^{-1}, which showed that all these compounds are salts. The presence of C=O peak at 1726 and 1723 cm^{-1} in **4** indicates the formation of co-crystal. Scheme 3 shows different heretosynthon involved in the structure of the salts and co-crystal. The crystallographic data and structure refinement parameters are given in Table 1. The selected hydrogen bonding data are summarized in Table 2.

Salt **1**, crystallizes in the monoclinic crystal system with $P2_1/c$ space group. The asymmetric unit contains one protonated $Pz^{Me2}H_2^+$ and one H_2BTC^- anion bonded

together through a variety of hydrogen bonds (Fig. 1 and S1). Six molecule of H_2BTC^- forms two (horizontal and vertical) types of cavities along *a* axis, each accommodating two molecules of $Pz^{Me2}H_2^+$ and forms a herringbone network (Fig. 2 & S2). The cyclic motif is comprised of two acid homodimers synthon I, and four trimeric heterosynthons IV with a cavity size 19.4 x 8.2 Å. In two dimensions, the sheet structure is formed which comprised of BTC molecules with inclusion of pyrazoles in the cavities. In three dimensions, these cavities, with a slight offset, aligned to form channels containing $Pz^{Me2}H_2^+$ (Fig. S3). The π···π interactions (π···π, 3.830(6) Å) between BTC and pyrazole results in the formation of three dimensional packing of the layers and these are the only interactions which stabilized the three dimensional packing in the crystal.

Salt **2** crystallizes in the triclinic crystal system with $P\bar{1}$ space group and its ORTEP view is shown in Fig.S4 . The asymmetric unit of **2** contained one protonated ($Pz^{iPr2}H_2^+$), two BTC molecules [one ionic (H_2BTC^-) and one neutral (H_3BTC)] and a disordered water molecule. The cavity in salt **2** is slightly larger and some what more planer in comparison to salt **1**, to accommodate bulky diisopropyl substituted pyrazole (Fig. S5). The hexagonal motif is formed by four acid dimers, synthon I, and two heterosynthons V. The wall of two such hexagonal nets are connected together by $Pz^{iPr2}H_2^+$ molecule via N–H···O interactions to form a bilayer type motif. These bilayers are further connected to each other by water molecules via O–H···O interaction (O1W···O9, 2.847(32) Å) and formed a two dimensional network (Fig. S6). Finally, these layers pack on each other through overlapping with a slight offset and results in channels across the layers (along *a* axis). These channels are filled with $Pz^{iPr2}H_2^+$ in a perpendicular manner with respect to the plane of the cavity (Fig.3). The pyrazole molecules are not in the plane of the acid

layers as in case of **1** but protruded from the cavity, probably due to the presence of bulky isopropyl groups on the pyrazole ring. The dimensions of the cavity is 15.2 x 14.4 Å and both the pyrazoles with-in the cavity are connected to each other through C–H···π (3.116(8) Å) interactions. The π···π interaction also exists between BTC molecules (π···π, 3.729(4) Å) and is responsible for the separation of 3.312(5) Å between the layers.

Table 1 Crystal data and structure refinement parameters of salts and co-crystal

	1	**2**	**3**	**4**	**5**	**6**	**7**
Emprical formula	$C_{14}H_{14}N_2O_6$	$C_{26.83}H_{27.49}N_2O_{12.11}$	$C_{27.92}H_{30}N_2O_{12.06}$	$C_{19}H_{16}N_2O_6$	$C_{31}H_{28}N_2O_{12}$	$C_{40}H_{34}N_4O_7$	$C_{29}H_{30}N_4O_{13}$
Formula weight	306.27	571.80	586.54	368.34	620.55	682.71	642.57
Crystal system	Monoclinic	Triclinic	Triclinic	Monoclinic	Triclinic	Triclinic	Monoclinic
Space group	*P*21/*c*	*P* $\bar{1}$	*P* $\bar{1}$	*P*21/*c*	*P* $\bar{1}$	*P* $\bar{1}$	*P*21/*n*
a/ Å	3.8298(4)	10.122(2)	10.037(3)	9.525(3)	10.979(2)	7.9394(17)	15.056(2)
b/ Å	13.6659(13)	10.636(2)	10.936(3)	27.883(9)	11.020(2)	11.221(2)	13.1093(18)
c/ Å	26.168(2)	14.713(3)	14.655(4)	13.755(4)	14.010(3)	19.683(4)	15.2651(19)
β/ °	91.048(5)	105.650(11)	104.698(14)	107.856(16)	78.13(3)	92.516(7)	105.105(5)
V / Å^3	1369.3(2)	1456.8(5)	1489.1(7)	3477.2(19)	1620.7(6)	1738.7(6)	2908.9(7)
Z	4	2	2	8	2	2	4
D_{calc} (g cm^{-3})	1.486	1.304	1.308	1.407	1.272	1.304	1.467
μ/mm^{-3}	0.118	0.104	0.104	0.106	0.099	0.091	0.117
θ range/ °	2.77- 30.86	2.50- 27.00	2.34- 26.78	2.78- 28.45	2.88- 28.45	2.38-29.43	2.89-30.31
Reflections collected	22270	27518	25830	24658	32695	11248	42927
Independent reflections	2901	6146	5233	6129	7062	6132	5105
Parameters	203	375	384	496	408	465	434
GOF (F^2)	1.057	1.681	0.973	0.940	0.966	1.189	1.175
R_1; wR_2 [$I>2\sigma(I)$]	0.0446; 0.1262	0.0641; 0.1309	0.0569; 0.1611	0.0594; 0.1193	0.0531; 0.1479	0.0517; 0.1325	0.0776; 0.2056
R_1; wR_2 (all data)	0.0629; 0.1351	0.1109; 0.1429	0.0875; 0.1837	0.1354; 0.1713	0.0938; 0.1968	0.0747; 0.1713	0.0847; 0.2095

The asymmetric unit of **3** contained one molecule of protonated ($Pz^{tBu,iPr}H_2^+$), two molecules of BTC (H_3BTC and H_2BTC^-) along with one molecule of crystalline water (Fig. S7). As in **2**, here also the hexagonal motif (Fig. S8) is formed by four acid dimers, via., synthon I and two heterosynthons V. Topologically the structure is very similar to **2**.

Weak C–H···π (3.292(3) Å) interaction is also present in between the pyrazole rings inside the hexagonal cavity (Fig. S9 & S10). Along with this, dipole–dipole interactions between the carbonyl groups of BTC (C=O···C, 3.233(7) Å) directs the three dimensional host guest packing as shown in figure 4.

The neutral co-crystal **4** crystallizes in the monoclinic crystal system with $P2_1/c$ space group and its ORTEP view is shown in Fig. S11. The asymmetric unit of **4** contained one molecule each of $Pz^{Ph,Me}H$ and H_3BTC, where no proton has been transferred from the acid to 3-phenyl-5-methylpyrazole base, which is also supported by the IR spectrum and the C=O bond lengths of BTC in the crystal structure. Both the components recognized each other through homosynthon I and neutral heterosynthon IV, resulted in a four membered roughly square shaped cavity of BTC (Fig. S12). Due to small size of cavities, the $Pz^{Ph,Me}H$ lies slightly outside the cavity and bonded to the carboxylic groups through heterosynthon IV. In salt **4**, the pyrazole with different substituents on 3 and 5 positions (phenyl and methyl), assembled themselves in such a way that the methyl groups from adjacent pyrazoles are facing to each other and the bulkier phenyl groups are close to each other, which results in the formation of two sets of cavities, one nearly square and other is rhomohedral in shape. One of the key features in the assembly is the slight deformation in one set of the cavities (A and B type) (Fig. 5). Methyl groups does not posed any steric hindrance to each other, so one set of rings are nearly square, however the phenyl groups, facing each other, causes steric hindrance. In order to relieve that hindrance, they deviate slightly and results in a cavity of rhomohedral shape. The Cg···Cg distance between BTC and pyrazole is 3.662(4) Å (Fig. S13). Figure S14 shows the three dimensional packing of co-crystal **4**.

The asymmetric unit of salt **5** consists of a protonated $Pz^{Cum,Me}H_2^+$ and two molecules of BTC (H_3BTC and H_2BTC^-) (Fig. S15). Similar to **2** and **3**, the hexagonal motif in **5** is also formed by four acid dimmers via., synthon I, and two heterosynthons V. The structure of **5** is very similar to **2** and **3**, where the respective pyrazoles resides in the cavity formed by the guest BTC molecules (Fig. S16). In case of salt **2-3**, the pyrazole bonded bilayers of BTC are connected through water molecules, however in salt **5,** there is no water molecule in between the bilayers and are sustained through other intermolecular interactions viz., weak π···π, 4.066(6) Å, interactions between pyrazole and BTC (H_3BTC and H_2BTC^-) molecules and dipole–dipole interactions (C=O···C, 3.415(4) Å) (Fig. S17-S18). The presence of different non-covalent interactions resulted in cationic and anionic host-guest structure where the BTC (H_3BTC and H_2BTC^-) acts as a host and 3-cumenyl-5-methylpyrazole cation as a guest molecule (Fig. 6).

Salt **6,** crystallizes in the triclinic crystal system with $P\bar{1}$ space group. One molecule of H_2BTC^- and two molecules of 3,5-diphenylpyrazole [one neutral ($Pz^{Ph2}H$) and other protonated ($Pz^{Ph2}H_2^+$)] along with one molecule of methanol are present in the asymmetric unit of salt **6** (Fig. S19). The two crystallographically independent pyrazole molecules showed different twist angles of the phenyl rings from the plane of the pyrazole ring (4.11°, 10.36° and 18.09°, 34.36°). The higher rotational angles of phenyl rings in one of the pyrazole is to relieve the steric hindrance between the bulky phenyl rings and this is also the reason for the formation of the trimeric synthon III, which is just an expanded form of the heterodimer II and is formed by the insertion of one methanol molecule in the heterosynthon II. This is the only structure of BTC with pyrazole which does not have extended hydrogen bonded network responsible for the cavity formation

(Fig. S20 & S21). The continuous chain of BTC runs parallel on either side of the chain formed by the pyrazoles. The presence of bulkier phenyl substitution at 3 and 5 position on the pyrazole ring may be responsible for the larger separation between two parallel chain of BTC and results in the absence of a cavity (Fig. 7).[27] It is interesting to note that $Pz^{Ph2}H$ alone formed cyclic tetramer through N−H···N hydrogen bonds (Scheme 1).[28] But in the presence of BTC, two different mixed synthons i.e., one heterodimer II and other trimeric III along with homodimeric synthon I, constituted the discrete hexameric hydrogen bonded aggregate. These hexamers recognized each other through aromatic interactions among BTC-BTC (Cg···Cg, 3.594(3) Å) and pyrazole-BTC rings (Cg···Cg, 3.801(6) Å) which is responsible for the three dimensional packing of the crystal.

Salt **7,** crystallizes in the monoclinic crystal system with $P2_1/n$ space group. Its asymmetric unit consists of a doubly protonated $BPzH_4^{2+}$, two molecules of H_2BTC^- and a methanol molecule (Fig. S22). Structural analysis revealed that six BTC molecules form brick wall type network (Fig. S23) along the *c* axis, with a cavity of dimension 16.2 x 9.4 Å which is quiet similar to the structure reported by Saha et al..[21] Two cationic $BPzH_4^{2+}$ and the methanol molecule adjust themselves in the cavity formed by the anionic carboxylate anion. Two homodimers, synthon I and four heterosynthons V are involved in the construction of the rectangular net. Two such rectangular networks were held together by $BPzH_2$ molecules through N–H···O type interactions via. synthon V, to form a bilayer. These bilayers are further stabilized by aromatic interactions between BTC molecules, (Cg···Cg, 3.636(4) Å) to form a three dimensional network (Fig. S24). Molecules of second layer mask the void space formed in one layer, i.e., they overlap each other partially (Fig. 8). The presence of different non-covalent interactions resulted

in host-guest structure, where the anionic host assembly was present with hexagonal cavity formed by the BTC molecules and the cationic guest pyrazole molecules are located inside the cavity (Fig. 9).

Comparing all the above supramolecular architecture, it was observed that H_3BTC molecule form cyclic cavities of varied dimensions with different substituted pyrazoles and formed host-guest type assemblies. H_3BTC formed six membered cyclic cavity with pyrazoles as guests viz., $Pz^{Me2}H$, $Pz^{iPr2}H$, $Pz^{tBu,iPr2}H$, $Pz^{Cum,Me}H$ and $BPzH_2$, while in case of co-crystal **4**, H_3BTC form four membered cavity (Fig. 10). In case of salt **6,** completely different packing was observed, the cavity completely disappears and chain of $Pz^{Ph2}H_2^+$ runs parallel on either side of the channel formed by the H_2BTC^-. From these structures it can be concluded that phenyl groups on the pyrazole does not favor the cavity formation of BTC while alkyl groups are helping in the formation of such assemblies. Also the ratio of both the component in the asymmetric unit also plays a significant role in dictating the shape of the cavity. In case of salt **6** the acid-pyrazole ratio is 1:2 unlike to the other cases where we found either 1:1 or 2:1 ratio. As a result, due to the presence of large number of –COOH groups in **1-5** and **7** as compared to the pyrazole, acid-acid bonding forms extended network. But this type of extension did not occur in **6**. This may be the reason why the acid molecules do not form cavity in **6**. It is important to point out that in all the structure host-guest type assemblies were formed with different size of cavity. It is also important to mention that different substituents on pyrazole rings controls the size of the cavity and also the shape and size of the cavity depends on the orientation of the molecule as well as short range interactions among them.

Table 2 Selected hydrogen bond parameters (Å, °) for salts and co-crystal 1.

D-H···A	d(D-H)	d(H···A)	d(D···A)	<(DHA)
O3–H3···O4 #1	0.821(1)	1.820(2)	2.632(3)	170
O5–H5···O1 #2	0.821(2)	1.794(4)	2.614(5)	178
N1–H1···O6 #3	0.860(2)	2.054(5)	2.838(7)	151
N2–H2···O2 #4	0.860(2)	1.685(1)	2.534(2)	168

Symmetry transformations used to generate equivalent atoms:
#1 -x+2, -y+1, -z+1 #2 -x+1, y-1/2, -z+1/2 #3 x+1, y, z #4-x+2, y-1/2, -z+1/2

2.

D-H···A	d(D-H)	d(H···A)	d(D···A)	<(DHA)
O2–H2A···O8 #1	0.820(5)	1.809(11)	2.617(16)	168
O3–H3···O11 #2	0.821(4)	1.800(9)	2.611(13)	169
O6–H6A···O9 #3	0.820(5)	1.638(11)	2.455(16)	173
O7–H7···O1 #4	0.820(6)	1.805(11)	2.617(16)	170
O12–H12···O4 #5	0.819(4)	1.821(9)	2.627(13)	167
N1–H1···O5 #6	0.860(6)	1.901(6)	2.694(12)	152
N2–H2B···O10 #7	0.859(6)	1.839(12)	2.611(18)	159

Symmetry transformations used to generate equivalent atoms:
#1 x+1, y, z #2 x, y+1, z #3 x, y, z-1 #4 x-1, y, z #5 x, y-1, z #6 x, y, z+1 #7 -x+2, -y+1, -z+2

3.

D-H···A	d(D-H)	d(H···A)	d(D···A)	<(DHA)
O2–H2B···O11 #1	0.820(7)	1.647(14)	2.463(20)	173
O4–H4A···O9 # 2	0.820(7)	1.824(13)	2.628(20)	166
O6–H6···O8	0.820(6)	1.813(12)	2.626(18)	171
O10–H10···O3 #3	0.820(7)	1.816(13)	2.624(20)	168
$N1^{+}$–H1···O12 #4	0.860(8)	1.860(14)	2.672(22)	156
N2–H2A···O1 #5	0.860(7)	1.897(9)	2.703(16)	155

Symmetry transformations used to generate equivalent atoms:
#1 x, y-1, z-1 #2 x+1, y-1, z #3 x-1, y+1, z #4 x-1, y, z-1 #5 -x+1, -y+1, -z

4.

D-H···A	d(D-H)	d(H···A)	d(D···A)	<(DHA)
O1–H1···O12 #1	0.820(4)	1.897(10)	2.671(13)	156
O6–H6···O9 #2	0.821(2)	1.820(2)	2.619(3)	164
O7–H7···O4 #3	0.819(4)	1.931(7)	2.748(10)	174
O10–H10···O5 #4	0.819(2)	1.881(2)	2.690(3)	169
O11–H11···N1 #5	0.821(4)	1.833(4)	2.602(7)	155
O3–H3···N4	0.819(4)	1.782(6)	2.598(9)	174
N2–H2···O2 #6	0.861(3)	1.994(4)	2.847(7)	170
N3–H3A···O8 #6	0.861(2)	1.003(5)	2.784(5)	150

Symmetry transformations used to generate equivalent atoms:
#1 x, y, z+1#2-x+1, y+1/2, -z+1/2 #3 x,-y+1/2, z+1/2 #4 -x+1, y-1/2, -z+1/2#5 x+1, y, z #6 x, -y+1/2, z-1/2

5.

D-H···A	d(D-H)	d(H···A)	d(D···A)	<(DHA)
O1–H1···O12 #1	0.821(11)	1.904(25)	2.724(36)	178
O5–H5···O9 #2	0.820(13)	1.866(31)	2.681(43)	172
O7–H7···O4 #3	0.820(14)	1.717(31)	2.534(44)	173
O10–H10···O6 #4	0.819(12)	1.903(32)	2.715(44)	170
O11–H11···O2 #5	0.821(10)	1.860(23)	2.681(34)	178
$N1^{+}$–H1A···O3 #6	0.860(15)	1.947(33)	2.735(46)	151
N2–H2A···O8 #7	0.860(2)	1.913(44)	2.772(63)	177

Symmetry transformations used to generate equivalent atoms:
#1 x+1, y, z+1 #2 x, y-1, z+1 #3 x-1, y+1, z #4 x, y+1, z-1 #5 x-1, y, z-1 #6 x-1, y+1, z #7 -x, -y+2, -z+1

6.

D-H···A	d(D-H)	d(H···A)	d(D···A)	<(DHA)
O7–H7···N2 #1	0.819(4)	1.950(8)	2.766(11)	173
N1–H1···O1 #2	0.860(3)	1.890(6)	2.733(8)	166
$N3^{+}$–H3---O4 #3	0.860(3)	1.935(7)	2.695(11)	146
N4–H4A···O3 #3	0.859(4)	2.058(8)	2.762(10)	138

Symmetry transformations used to generate equivalent atoms:
#1 -x+1, -y+1, -z+1 #2 -x, -y+1, -z+1 #3 x, y, z-1

7.

D-H···A	d(D-H)	d(H···A)	d(D···A)	<(DHA)
O1–H1···O8 #1	0.820(3)	1.764(6)	2.560(6)	166
O9–H9···O3 #2	0.819(3)	1.627(4)	2.437(6)	169
O5–H5···O12 #3	0.820(3)	1.692(4)	2.505(6)	170
O7–H7···O2 #1	0.820(3)	1.790(5)	2.603(6)	171
O13–H13···O6 #4	0.819(5)	2.060(3)	2.842(6)	157
N1–H1B···O10	0.785(48)	1.860(45)	2.620(4)	164
$N2^{+}$–H2B···$O11^{-}$ #5	0.860(3)	1.786(3)	2.621(4)	163
N3–H3A···O12 #6	0.920(51)	1.817(50)	2.725(6)	169
$N4^{+}$–H4A···$O4^{-}$ #7	0.859(4)	1.994(3)	2.672(4)	134

Symmetry transformations used to generate equivalent atoms:
#1 -x+2, -y+1, -z #2-x+2, -y+1, -z+1 #3 -x+1, -y+1, -z #4 -x+3/2, y-1/2, -z+1/2#5 x+1/2 ,-y+1/2, z+1/2 #6 x, y, z+1 #7 -x+3/2, y-1/2, -z+3/2

Theoretical studies

The optimized structural parameters of all individual acid, pyrazoles and their salts were calculated at B3LYP/6-31G(d, p) basis sets. Each optimized geometry showed positive vibrational frequencies suggesting that the optimized structure was the global minimum on the potential energy surface (Fig. 11). Single point energy calculations were

performed and zero point corrected total energies for various species were recorded. The hydrogen bond interaction energies were determined using the following equation,

$\Delta E = E_{Salt} - (E_{Pyrazole} + E_{Acid})$

Where E_{Salt} , $E_{Pyrazole}$ and E_{Acid} are the zero point corrected total energies of salt, pyrazole and acid. We have removed the solvent and water molecules to check the relative stability. The interaction energies (IE) for salts and co-crystals are tabulated in Table 3. In all the cases, except **4**, the proton transfer reaction was observed in the solid state but in gaseous phase such type of reaction was not observed indicating that structures in both the solid and gaseous phase are not same. The interaction energies in salt **1**-**3** increases with the increase of electron donating groups on pyrazole ring. The proton preferably binds to the lone pair of nitrogen present in the plane of the ring. The presence of higher substitution makes the pyrazole ring more and more electron rich thereby increases the interaction energies, i.e., greater is the electron donating ability, larger will be the interaction energy.[29] The interaction energy decreases in co-crystal **4**, because of the presence of phenyl group, which is weak electron withdrawing in nature. In case of salt **5**, the interaction energy again increases due to the presence of electron donating nature of isopropyl group attached to the phenyl ring. In case of salt **6**, due to the two phenyl groups (electron withdrawing) on pyrazole, the interaction energy was decreased. The presence of four methyl group on the H_2BPz is responsible for the increase in the interaction energy.

Synthon evaluation

To evaluate the robustness of the synthons in these complexes DFT calculation was done on the two dimer synthons to find out their energies of formation, which is summarized in

Table 4. Energy calculation shows that the acid homodimer $\mathbf{R^2_2(8)}$ {I} is more energy stabilized as compared to acid-base heterodimer $\mathbf{R^2_2(7)}$ {II} and therefore $\mathbf{R^2_2(8)}$ is responsible for its frequent occurrence in most of the structures (Fig. 12). A correlation can be made based on the substituents of pyrazole and the occurrence of synthons in these salts and co-crystal (Table 5). Pyrazole with atleast one methyl group always form heterosynthon IV and pyrazoles having isopropyl group exceptionally form synthon V with the carboxylic acids.

Table 3 Hydrogen bond interaction energy (**1-7**) (Kcal/mol)

S.No.	Salt or Co-crystal of BTC	Hydrogen bond interaction energy (Kcal/mol)
1	**1**	-19.829
2	**2**	-19.892
3	**3**	-19.993
4	**4**	-19.390
5	**5**	-19.453
6	**6**	-18.762
7.	**7**	-19.966

Table 4 Synthon Energies (Kcal/mol)

S.No.	Synthon	Energy (Kcal/mol)
1	Acid-Acid homodimer $\mathbf{R_2^2(8)}$ (**i**)	-20.143
2	Acid-Pyrazole heterodimer $\mathbf{R_2^2(7)}$ (**ii**)	-18.762

Table 5 Occurrence of synthons in salts and co-crystal

	$Pz^{Me2}H$	$Pz^{iPr2}H$	$Pz^{tBu,iPr}H$	$Pz^{Ph,Me}H$	$Pz^{Cum,Me}H$	$Pz^{Ph2}H$	$BPz\ H_2$
BTC	**i & iv**	**i & v**	**i & v**	**i & iv**	**i & v**	**i, ii & iii**	**i & v**

Thermal analysis

To study the thermal stability of the salts and co-crystal, thermo-gravimetric analysis (TGA) was performed. TGA curves of different pyrazoles with H_3BTC (**1-7**)

were compared in Fig. S25. Comparison of TGA curves indicated that **7** (234 ºC) is the most stable, due to the presence of highest number of interactions. All the complexes showed the mass loss in similar fashion, the first mass loss relates to the expulsion of solvent molecule. Second step is the decarboxylation process of the COOH group and the third & final step is the thermal decomposition of the remaining organic residue. Salt **6** is the least stable complex which may be due to the collapse of cavities and less number of interactions.

Powder XRD

We also examined the structural homogeneity of bulk samples of salts or co-crystal through a comparison of experimental and simulated powder X-ray diffraction (XRD) patterns. The experimental patterns correlate favorably with the simulated ones generated from single-crystal X-ray diffraction (Fig. S26).

Conclusion

We have reported the synthesis and rational analysis of supramolecular assemblies formed by H_3BTC with various substituted pyrazoles. In all cases the proton has been transferred from H_3BTC to the pyrazole and resulted in cationic anionic pair (salt) except in case of $Pz^{Ph,Me}H$. There is no proton transfer with $Pz^{Ph,Me}H$ and the formation of a co-crystal occurred. In all co-crystal and salt, due to various non-covalent interactions, the host H_3BTC molecule form cavity of different size for different substituted guest pyrazole molecules except in **6**, where the chain of cationic pyrazole molecules are sandwiched in between the channels of the anionic BTC molecules. Synthon energies of the homo and heterodimers were calculated to evaluate their occurrence in the solid states and found that acid homodimer $\mathbf{R^2_2(8)}$ is more energy

stabilized in comparison to the acid-pyrazole heterodimer $\mathbf{R^2_2(7)}$ and that is why $\mathbf{R^2_2(8)}$ acid homodimer is invariably present in almost all the structures. The trend observed for the interaction energy suggest that the co-crystals or salts with higher number of electron donating group (with +I effect) have higher interaction energy and vice-versa. Thermal study showed that the salt of $BPzH_2$ is most stable probably due to the presence of more number of interactions.

Experimental

General

All manipulations were performed in air using commercial grade solvents, predried by the literature method.[30] 3,5-diisopropylpyrazole ($Pz^{iPr2}H$), 3-tert-butyl-5-isopropylpyrazole ($Pz^{tBu,iPr}H$), 3-phenyl-5-methylpyrazole ($Pz^{Ph,Me}H$), 3-cumenyl-5-methylpyrazole ($Pz^{Cum,Me}H$) and 3,5-diphenylpyrazole ($Pz^{Ph2}H$) and 3,3′,5,5′-tetramethyl-4,4′-bipyrazole ($BPzH_2$) were prepared by literature method.[11,31] Benzene-1,3,5-tricarboxylic acid (H_3BTC) and 3,5-dimethylpyrazole ($Pz^{Me2}H$) were purchased from Aldrich Chemical Company, USA. Crystallized salts or co-crystal were carefully dried under vacuum prior to elemental analysis on Elementar Vario EL III analyzer. IR spectra were obtained on a Thermo Nikolet Nexus FT-IR spectrometer in KBr pellets. The thermal analyses were performed on Perkin-Elmer's (Pyris Diamond) thermogravimetry analyzer under air atmosphere. Powder XRD data were collected using Bruker Advance D8 XRD diffractometer.

Synthetic procedure for complexes 1-7

$[H_2BTC^-.Pz^{Me2}H_2^+]$ **(1)**

An aqueous-methanolic (10 mL) solution of H_3BTC (0.21 g, 1.00 mmol) and $Pz^{Me2}H$ (0.09 g, 1.00 mmol) in 1:1 mole ratio was heated for 30 min. The resultant colorless solution was filtered and allowed to stand at room temperature. Colorless block shaped crystals of salt **1** were obtained by slow evaporation of the solvent in 76% (0.23 g, 0.76 mmol) yield. Anal Calc. for $C_{14}H_{14}N_2O_6$: C, 54.90; H, 4.61; N, 9.15 %. Found: C, 54.16; H, 4.53; N, 9.03 %. IR (KBr, cm^{-1}): 3262, 2928, 2437, 1832, 1684, 1584, 1454, 1354, 1261, 1179, 1138, 1096, 862, 659.

$[H_3BTC.H_2BTC^-.Pz^{iPr2}H_2^+.H_2O]$ **(2)**,

Salt **2** was prepared by the method employed for **1** using $Pz^{iPr2}H$ (0.15 g, 1.00 mmol). Yield: 64.4% (0.19 g, 0.64 mmol). Anal Calc. for $C_{27}H_{28}N_2O_{13}$: C, 56.10; H, 4.80; N, 4.76 %. Found: C, 56.22; H, 4.68; N, 4.72 %. IR (KBr, cm^{-1}): 3083, 2847, 2647, 1700, 1608, 1572, 1455, 1217, 1179, 1077, 963, 765, 644, 510.

$[H_3BTC.H_2BTC^-.Pz^{tBu,iPr}H_2^+.H_2O]$ **(3)**

Salt **3** was prepared by the method employed for **1** using $Pz^{tBu,iPr}H$ (0.17 g, 1.00 mmol). Yield: 58 % (0.17 g, 0.58 mmol). Anal Calc. for $C_{28}H_{30}N_2O_{13}$: C, 55.63; H, 5.34; N, 4.63 %. Found: C, 55.37; H, 5.26; N, 4.48 %. IR (KBr, cm^{-1}): 3420, 3056, 2801, 2442, 1923, 1707, 1614, 1567, 1423, 1205, 1097, 891, 677, 619, 512.

$[H_3BTC.Pz^{Ph,Me}H]$ **(4)**

Co-crystal **4** was prepared by the method employed for **1** using $Pz^{Ph,Me}H$ (0.16 g, 1.00 mmol). Yield: 72% (0.26 g, 0.72 mmol). Anal Calc. for $C_{19}H_{16}N_2O_6$: C, 62.95; H, 4.38; N, 7.61 %. Found: C, 62.84; H, 4.26; N, 7.52 %. IR (KBr, cm^{-1}): 3201, 3034, 2875, 2604, 1726, 1693, 1596, 1484, 1257, 1100, 929, 800, 744, 605, 586.

$[H_3BTC.H_2BTC^-.Pz^{Cum,Me}H_2^+]$ **(5)**

Salt **5** was prepared by the method employed for **1** using $Pz^{Cum,Me}H$ (0.20 g, 1.00 mmol). Yield: 74% (0.23 g, 0.74 mmol). Anal Calc. for $C_{31}H_{28}N_2O_{12}$: C, 60.00; H, 4.55; N, 4.51 %. Found: C, 60.16; H, 4.44; N, 4.40 %. IR (KBr, cm^{-1}): 3347, 3076, 2965, 2852, 1696, 1589, 1503, 1461, 1423, 1366, 1205, 1165, 1031, 986, 808, 644, 594.

$[H_2BTC^-.Pz^{Ph2}H_2^+.Pz^{Ph2}H.CH_3OH]$ **(6)**

Salt **6** was prepared by the method employed for **1** using $Pz^{Ph2}H$ (0.22 g, 1.00 mmol). Yield: 82% (0.28 g, 0.82 mmol). Anal Calc. for $C_{40}H_{34}N_4O_7$: C, 70.37; H, 5.02; N, 8.21 %. Found: C, 70.24; H, 5.11; N, 8.10 %. IR (KBr, cm^{-1}): 3552, 3085, 2852, 2656, 2548, 1716, 1606, 1564, 1456, 1403, 1280, 1185, 1075, 971, 806, 761, 681, 521.

$[2H_2BTC^-.BPzH_4^{2+}.CH_3OH]$ **(7)**

Salt **7** was prepared by the method employed for **1** using $BPzH_2$ (0.19 g, 1.00 mmol)**.** Yield: 74.7 % (0.24 g 0.74 mmol). Anal Calc. for $C_{29}H_{30}N_4O_{13}$: C, 54.21; H, 4.71; N, 8.72 %. Found: C, 54.13; H, 4.59; N, 8.60 %. IR (KBr, cm^{-1}): 3195, 3079, 2917, 2556, 1696, 1456, 1361, 1299, 1173, 1016, 900, 785, 619, 520.

X-ray crystal structure determination

The X-ray data collection were performed on a Bruker Kappa Apex four circle-CCD diffractometer using graphite monochromated MoKα radiation (λ = 0.71070 Å) at 100 K. In the reduction of data Lorentz and polarization corrections, empirical absorption corrections were applied.[32] Crystal structures were solved by Direct methods. Structure solution, refinement and data output were carried out with the SHELXTL program.[33-34] Non-hydrogen atoms were refined anisotropically. Hydrogen atoms were placed in geometrically calculated positions by using a riding model. Images and hydrogen

bonding interactions were created in the crystal lattice with DIAMOND and MERCURY software. [35-36]

Computational Study

Geometry optimization of different species involved during the course of present investigation were done using Density Functional Method (B3LYP) with 6-31G(d,p) basis set as implemented in the Gaussian 03 suite of program.[37-38] The input for the simulation was the z-matrix generated by Gauss view [39] that was also used for visualizing the optimized structures of molecules. ChemCraft, version 1.5 software was used for comparing the optimized structure with the crystallographic one.

Acknowledgment

The authors gratefully acknowledge CSIR, New Delhi, India for financial assistance.

Supporting Information Available: Crystal data in CIF format. This material is available free of charge via the internet.

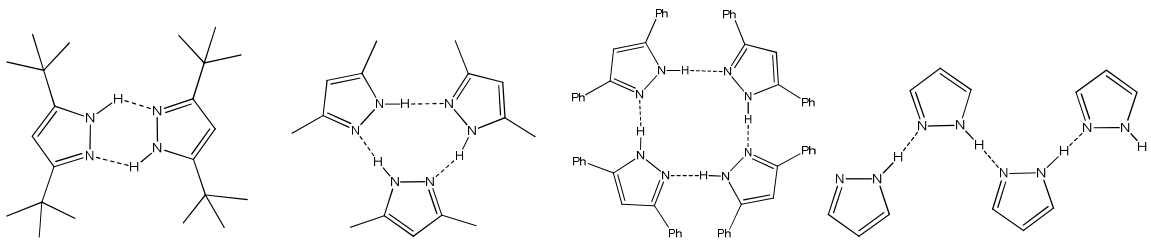

$Pz^{tBu2}H$ (Dimer) $Pz^{Me2}H$ (Trimer) $Pz^{Ph2}H$ (Tetramer) PzH (Catemer)

Scheme 1 Homosynthons of some substituted pyrazoles

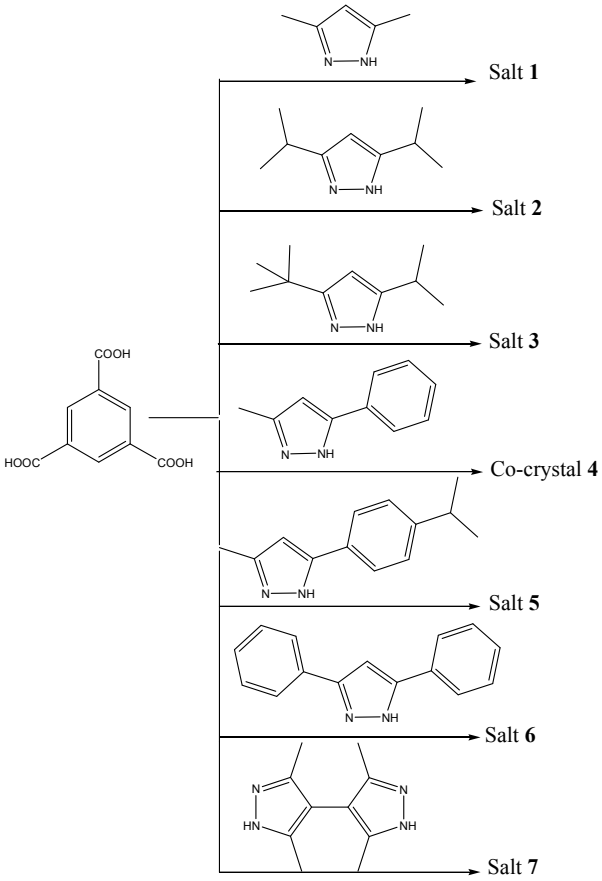

Scheme 2

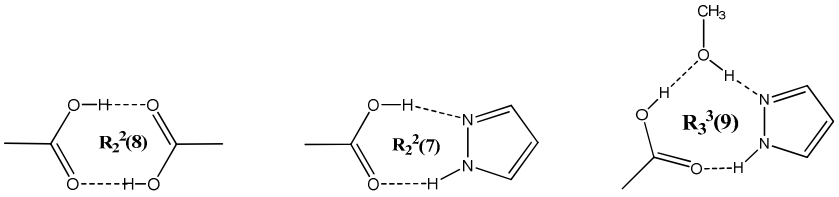

I II III

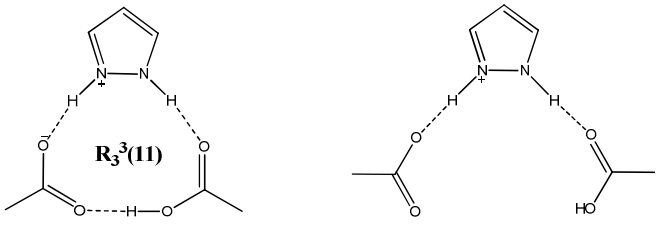

IV V

Scheme 3 Observed homo and hetero synthons in salts and co-crystal

References:

1. (a) G. R. Desiraju, *Crystal Engineering*: *The Design of Organic Solids*, Elsevier: Amsterdam, 1989; (b) G. R. Desiraju, *Angew. Chem., Int. Ed.*, 1995, **34**, 2311–2327.
2. (a) C. B. Aakeroy, A. M. Beatty and B. A. Helfrich, *Angew. Chem., Int. Ed.*, 2001, **40**, 3240-3242; (b) T. Steiner, *Angew. Chem.*, *Int. Ed.* 2002, **41**, 48–76.
3. (a) C. Lopez, R. M. Claramunt, M. A. García, E. Pinilla, M. R. Torres, I. Alkorta and J. Elguero, *Cryst. Growth Des.*, 2007, **7**, 1176–1184; (b) P. Krogsgaard-Larsen, T. Liljefors and U. Madsen, *Eds*. *Textbook of Drug Design and Discovery*, 3rd ed., Taylor and Francis: New York, 2002.
4. H. W. Ehrlich, *Acta Cryst.*, 1960, **13**, 946–952.
5. A. Baldy, J. Elguero, R. Faure, M. Pierrot and E. J. Vincent, *J. Am. Chem. Soc.*, 1985, **107***,* 5290–5291.
6. F. Aguilar-Parrilla, H. H. Limbach, C. Foces-Foces, F. H. Cano, N. Jagerovic and J. Elguero, *J. Org. Chem.*, 1995, **60**, 1965–1970.
7. F. Aguilar-Parrilla, G. Scherer, H. H. Limbach, C. Foces-Foces, F. H. Cano, J. A. S. Smith, C. Toiron and J. Elguero, *J. Am. Chem. Soc.*, 1992, **114**, 9657–9659.
8. I. Alkorta, J. Elguero, B. Donnadieu, M. Etienne, J. Jaffart, D. Schagen and H. H. Limbach, *New J. Chem*., 1999, **23**, 1231–1237.
9. R. S. Claramunt, J. Elguero, C. Foces-Foces, A. L. Llamas-Saiz, F. Aguilar-Parrilla, O. Klein and H. -H. Limbach, *J. Chem. Soc., Perkin Trans.*, 1997, **2**, 1867–1876.

10. C. Foces-Foces, A. Echevarría, N. Jagerovic, I. Alkorta, J. Elguero, U. Langer, O. Klein, M. Minguet-Bonvehí and H. -H. Limbach, *J. Am. Chem. Soc*., 2001, **123**, 7898–7906.

11. I. Boldog, E. B. Rusanov, A. N. Chernega, J. Sieler and K. V. Domasevitch, *Angew. Chem., Int. Ed*., 2001, **40**, 3435–3438.

12. E. B. Rusanov, V. V. Ponomarova, V. V. Komarchuk, H. S. Evans, E. F. Ibanez, F. Stoeckli, J. Sieler and K. V. Domasevitch, *Angew. Chem., Int. Ed*., 2003, **42**, 2499–2501.

13. I. Boldog, E. B. Rusanov, J. Sieler and K. V. Dommasevitch, *New. J. Chem*., 2004, **28**, 756–759.

14. (a) T. Nyui, T. Nogamia and T. Ishida, CrystEngComm, 2005, 7, 612–615; (b) U. P. Singh, S. Kashyap, H. J. Singh and R. J. Butcher, CrystEngComm, 2011, **13**, 4110-4120; (c) U. P. Singh, S. Kashyap, R. J. Butcher, H. J. Singh and B. K. Mishra, Struct. Chem. 2011, **22,** 931-941 (2011).

15. H. Gong and M. J. Krische, *Angew. Chem. Int. Ed*., 2005, **44**, 7069 –7071.

16. (a) C. V. K. Sharma and M. J. Zaworotko, *Chem. Commun.* 1996, 2655–2656; (b) M. Du, Z. H. Zhang and X. J. Zhao, *Cryst. Growth Des.*, 2005, **5**, 1247–1254; (c) T. R. Shattock, P. Vishweshwar, Z. Wang and M. J. Zaworotko, *Cryst. Growth Des.*, 2005, **5**, 2046–2049; (d) D. J. Duchampand and R. E. Marsh, *Acta Crystallogr. Sect.*, *B* 1969, **25**, 5–19; (e) R. Santra, N. Ghosh and K. Biradha, *New J. Chem.*, 2008, **32**, 1673–1676; (f) R. Santra and K. Biradha, *Cryst. Growth Des*., 2009, **9**, 4969–4978; (g) R. Liu, K. Mok and S. Valiyaveettil, *New J. Chem*., 2001, **25**, 890–892; (h) P. Vishweshwar, D. A. Beauchamp and M. J. Zaworotko,

Cryst. Growth Des., 2006, **6**, 2429–2431. (i) I. Goldberg and J. Bernstein, *Chem. Commun*., 2007, 132–134. (j) L. Rajput, N. Jana and K. Biradha, *Cryst. Growth Des*., 2010, **10**(10), 4565–4570; (h) L. Rajput and K. Biradha, *Cryst. Growth Des*., 2009, **9**(1), 40–42; (k) R. Santra and K. Biradha, *Cryst. Growth Des*., 2009, **9**, 4969–4978.

17. E. H. Herbstein, M. Kapon and G. M. Reisner, *J. Inclusion Phenom.*, 1987, **5**, 211–214.
18. S. V. Kolotuchin, E. E. Fenlon, S. R. Wilson, C. J. Loweth and S. C. Zimmerman, *Angew. Chem. Int. Ed. Engl.*, 1995, **34**, 2654-2656.
19. R. E. Melendez, C. V. K. Sharma, M. J. Zaworotko, C. Bauer and R. D. Rogers, *Angew. Chem. Int. Ed. Engl*., 1996, **35**, 2213–2215.
20. B.-Q. Ma and P. Coppens, *Chem. Commun*., 2003, 2290–2291.
21. S. Bhattacharya and B. K. Saha, *Cryst. Growth Des.*, 2011, **11**, 2194–2204.
22. C. Foces-Foces, L. Infantes, F. Aguilar-Parrilla, N. S. Golubev, H. –H, Limbach and J. Elguero, *J. Chem. Soc., Perkin Trans.*, 1996, **2**, 349–353.
23. C. Lopez, R. M. Claramunt, M. A. García, E. Pinilla, M. R. Torres, I. Alkorta and J. Elguero, *Cryst. Growth Des*., 2007, 7, 1176–1184.
24. T. Basu, H. A. Sparkes and R. Mondal, *Cryst. Growth Des*., 2009, **9**, 5164–5170.
25. M. Arunachalam, S. Chakraborty, S. Marivel, and P. Ghosh, *Cryst. Growth Des*., 2012, **12**, 2097−2108.
26. (a) K. Biradha, D. Dennis, V. A. MacKinnon, C. V. K. Sharma and M. J. Zaworotko, *J. Am. Chem. Soc.,* 1998, **120***,* 11894–11903; (b) K. Biradha and M. J. Zaworotko, *Cryst. Eng*., 1998, **1**, 67–78; (c) K. K. Arora and V. R. Pedireddi,

J. Org. Chem., 2003, **68**, 9177–9185.; (d) O. Fabelo, L. C. Delgado, F. S. Delgado, P. L. Luis, M. M. Laz, M. Julve and C. R. Prez, *Cryst. Growth Des.,* 2005, **5**, 1163–1167; (e) K. K. Arora, M. S. Talwelkar and V. R. Pedireddi, *New. J. Chem*., 2009, **33**, 57–63.

27. J. A. Bis and M. J. Zaworotko, *Cryst. Growth Des*., 2005, 5, 1169–1179.
28. L. E. Cheruzel, M. S. Pometun, M. R. Cecil, M. S. Mashuta, R. J. Wittebort, and R. M. Buchanan, *Angew. Chem. Int. Ed.*, 2003, **42**, 5452–5455.
29. F. Aguilar-Parrilla, G. Scherer, H. H. Limbach, C. Foces-Foces, F. H. Cano, J. A. S. Smith, C. Toiron and J. Elguero, *J. Am. Chem. Soc.*, 1992, **114**, 9657–9659.
30. D. D. Perrin, W. L. Armarego and D. R. Perrin, *Purification of Laboratory Chemicals*,
Pergamon, New York, 2nd Edd. 1980.
31. S. Imai, K. Fujisawa, T. Kobayashi, N. Shirasawa, H. Fujii, T. Yoshimura, N. Kitajima and Y. Morooka, *Inorg. Chem*., 1998, **37,** 3066–3071; (b) N. Kitajima, K. Fujisawa, C. Fujimoto, Y. Morooka, S. Hashimoto, T. Kitagawa, K. Toriumi, K. Tatsumi and A. Nakamura, *J. Am. Chem. Soc*., 1992, **114**, 1277–1291.
32. G. M. Sheldrick, *SADABS*, University of Göttingen, Germany, 1996.
33. G. M. Sheldrick, *Acta Cryst.,* 1990, **A 46**, 467–473.
34. G. M. Sheldrick, *SHELXTL-NT 2000* version 6.12, reference manual, University of Göttingen, Göttingen, Germany.
35. K. Brandenburg, *Diamond*: *Visual Crystal Structure Information System* (Version 2.1d), Crystal Impact GbR, Bonn, Germany, 2000.

36. *Mercury*, Cambridge Crystallographic Data Centre, 12 Union Road, Cambridge CB2 1EZ, United Kingdom. Available from: Website: http://www.ccdc.cam.ac.uk/.

37. *Gaussian 03, Rev. C.02,* Gaussian, Inc., Wallingford CT, 2004.

38. P. C. Hariharan and J. A. Pople, *Theo. Chem. Acta,* 1972, **28**, 213–222.

39. A. Frisch, A. B. Nielsen and A. J. Holder, *Gauss View users Manual*, Gaussian Inc, Wallingford, CT, 2003.

Caption of figures

Fig. 1 ORTEP drawing with 50% probability of salt **1**.

Fig. 2 Herringbone network of H_3BTC (shown in space fill model) in **1**, where the cavities are filled with 3,5-diemthyl pyrazole molecules.

Fig. 3 Slightly offset arrangement of cavities in two layers of H_3BTC forming channels (green and blue) in space fill model filled with $Pz^{iPr2}H$ (Red color).

Fig. 4 Three dimensional packing of salt **3.** Guest pyrazole cations are entrapped in the cage formed by the host anionic H_3BTC assembly. Color code: BTC, red; $Pz^{tBu,iPr}H$, blue.

Fig. 5 Two types of cavities labeled as **A** and **B** (purple and cyan color). The close proximity of phenyl groups causes trimeric synthons.

Fig. 6 Three dimensional packing of salt **5.** Guest pyrazole cations are entrapped in the cavity of host BTC assembly. Color code: BTC, red; $Pz^{Cum, Me}H$, blue

Fig. 7 Alternate channels of host framework formed by the self-assembly of the anionic BTC molecules with guest pyrazole cations on both side in salt **6**. Color code: BTC, red; $Pz^{Ph2}H$, blue.

Fig. 8 Masking of cavities between two layers in **7** (green and blue colors).

Fig. 9 Brick-wall network of H_3BTC in salt **7**, $BPzH_2$ and methanol molecules are present in the cavities. Color code: $BPzH_2$, purple; CH_3OH, blue.

Fig. 10 An overall view of the host assembly formed the host H_3BTC molecule.

Fig. 11 Optimized geometry of salts and co-crystal.

Fig. 12 Optimized geometries of acid homo $R^2_2(8)$ **{I}** and acid-base heterosynthons $R^2_2(7)$ **{II}**

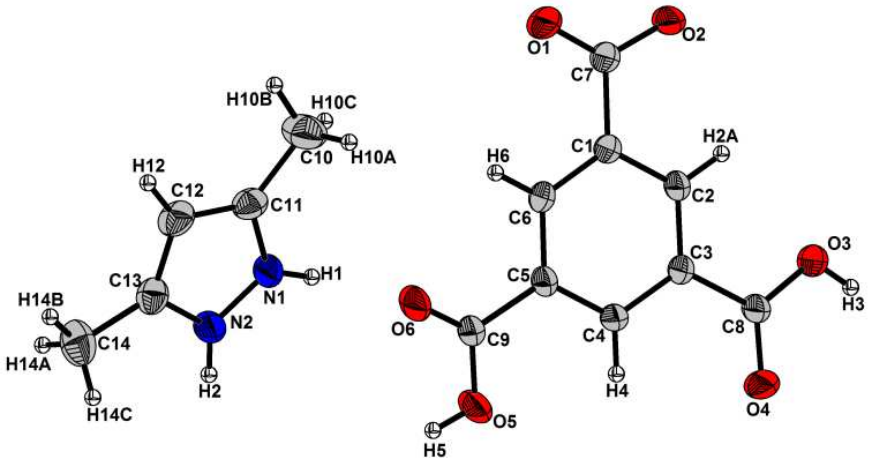
O1
O2
C7
H10B
H10C
C10
H10A
H12
C12
C11
C1
H2A
H6
C2
C6
C3
O3
C13
C5
H1
N1
H3
H14B
N2
O6
C9
C4
C8
C14
H14A
H4
O4
H14C
H2
O5
H5

Fig. 1

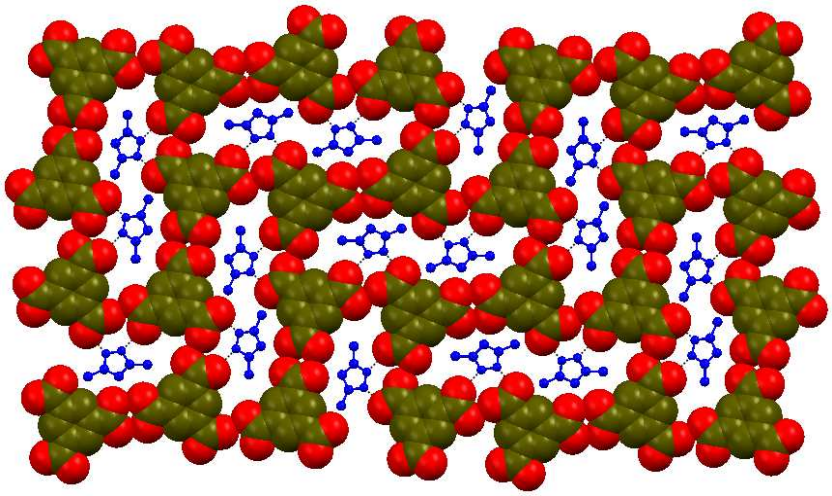

Fig. 2

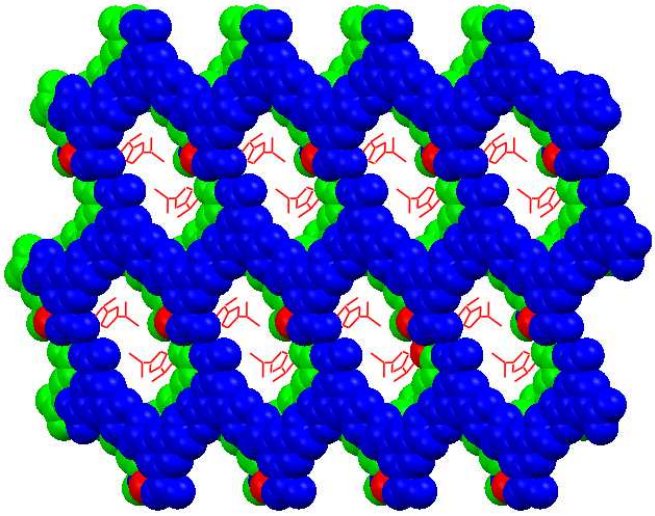

Fig. 3

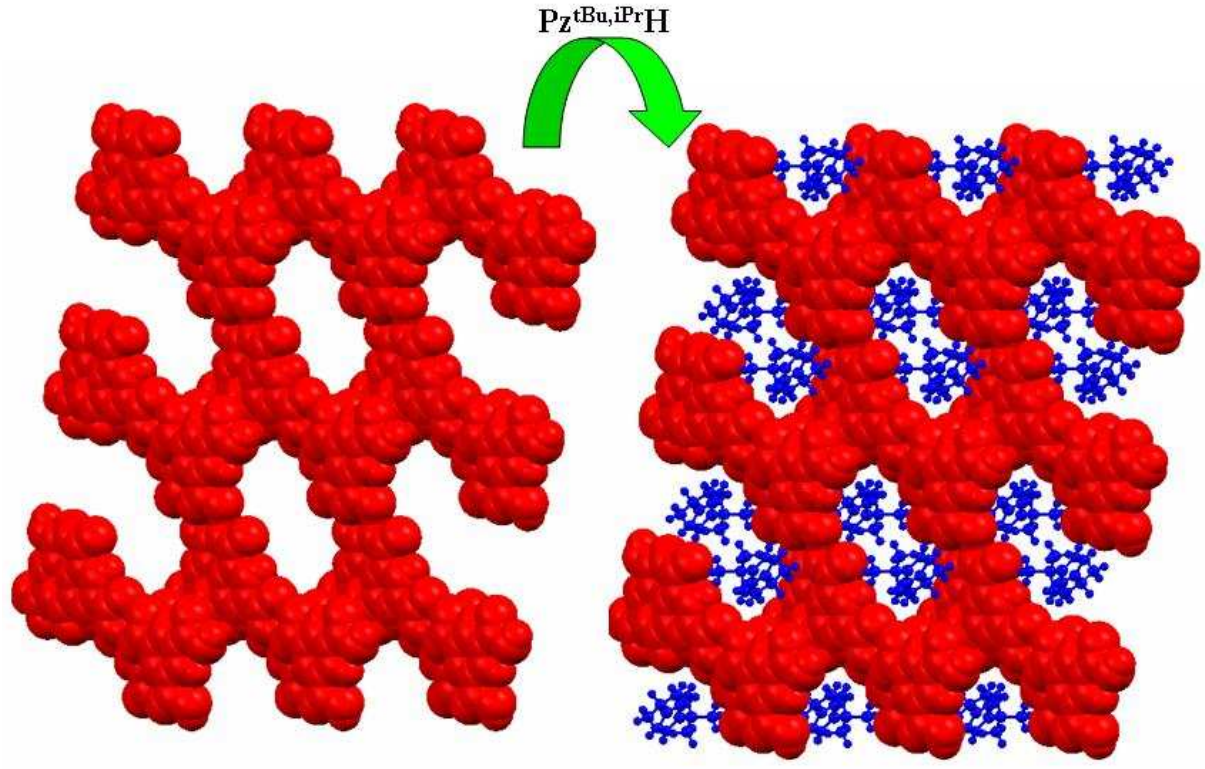

Fig. 4

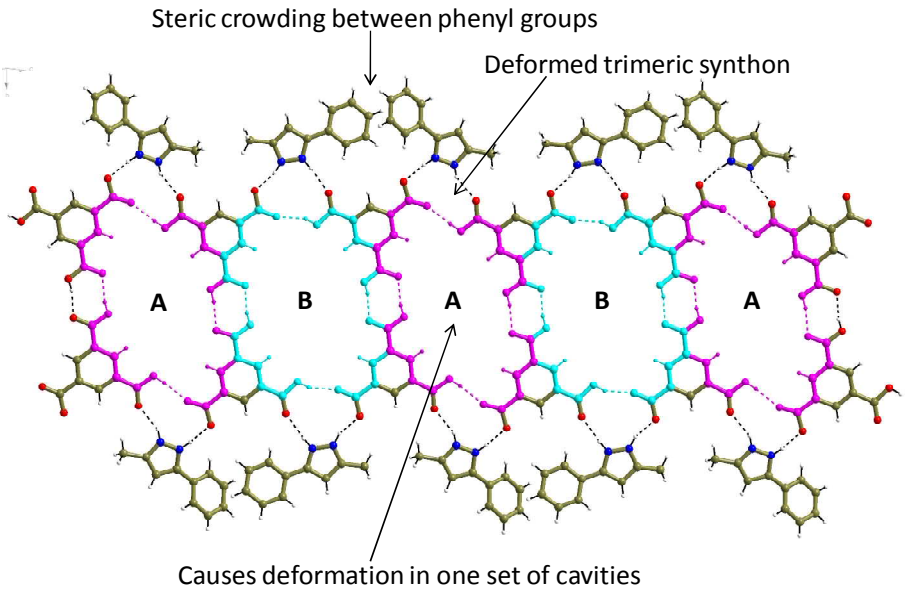
Steric crowding between phenyl groups
Deformed trimeric synthon
A
B
A
B
A
Causes deformation in one set of cavities

Fig. 5

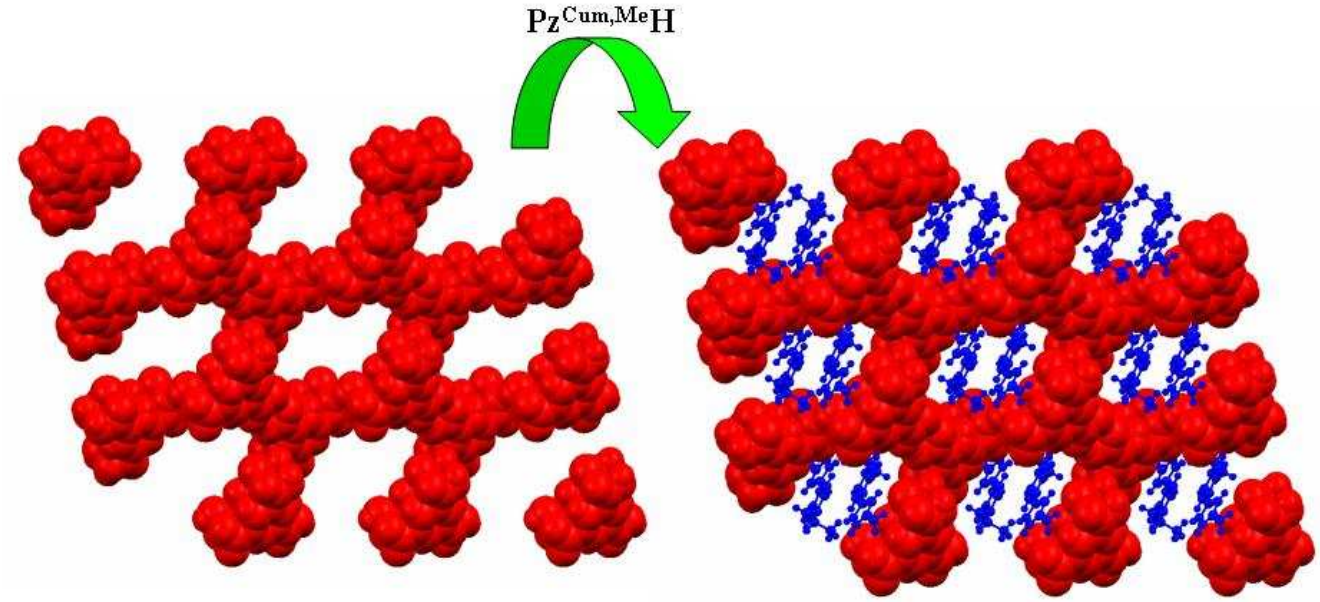
PzCum,MeH

Fig. 6

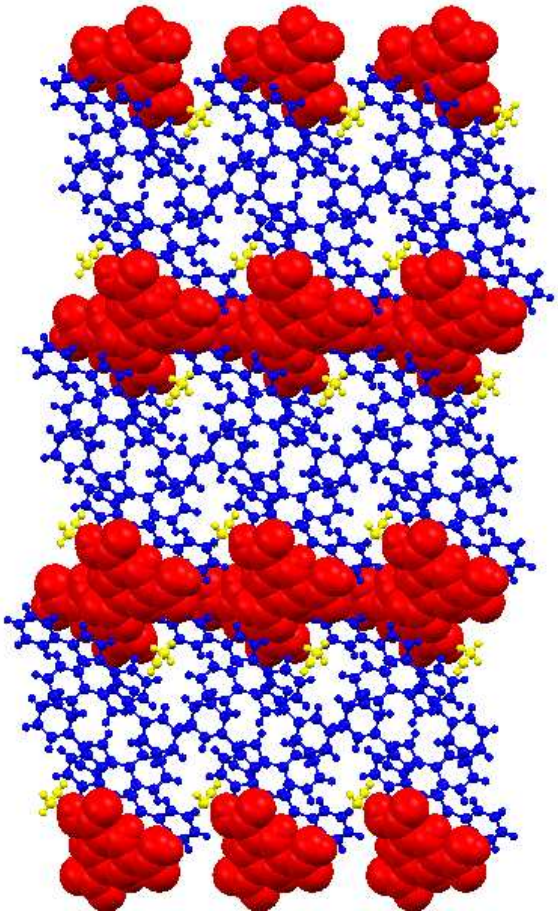

Fig. 7

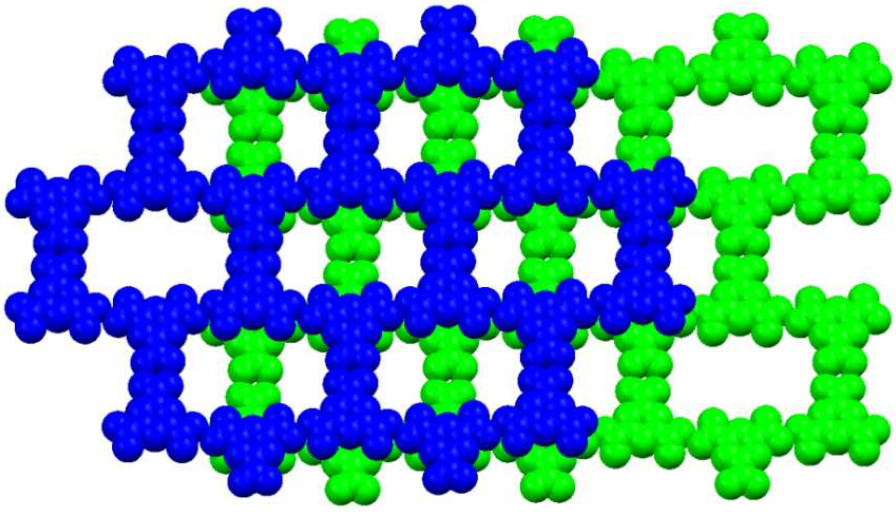

Fig. 8

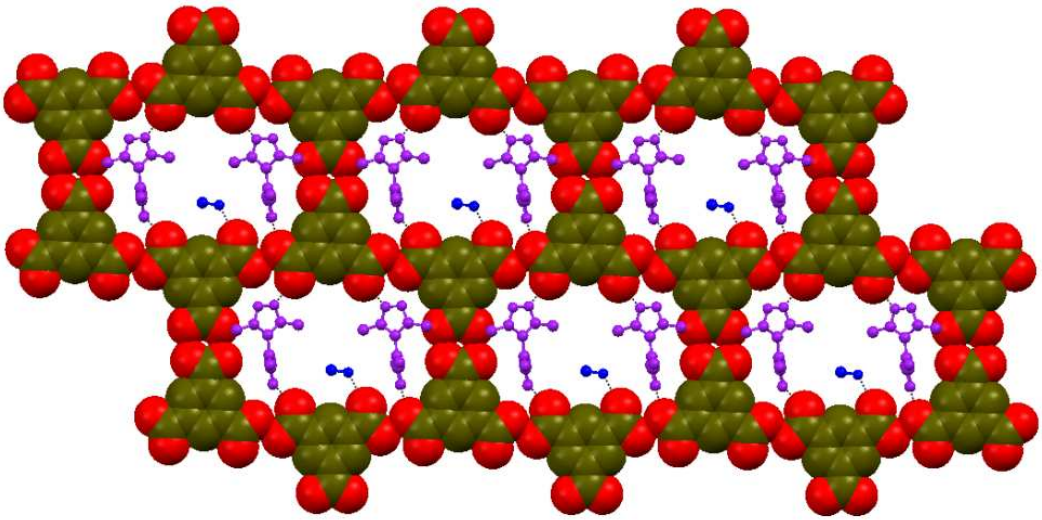

Fig. 9

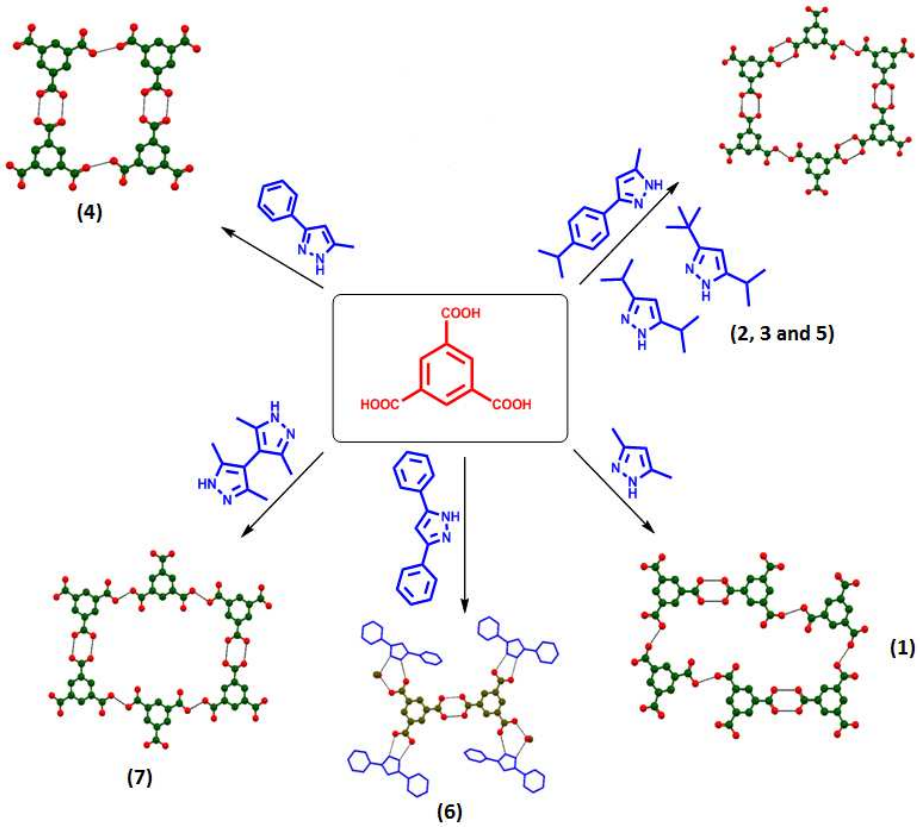

Fig. 10

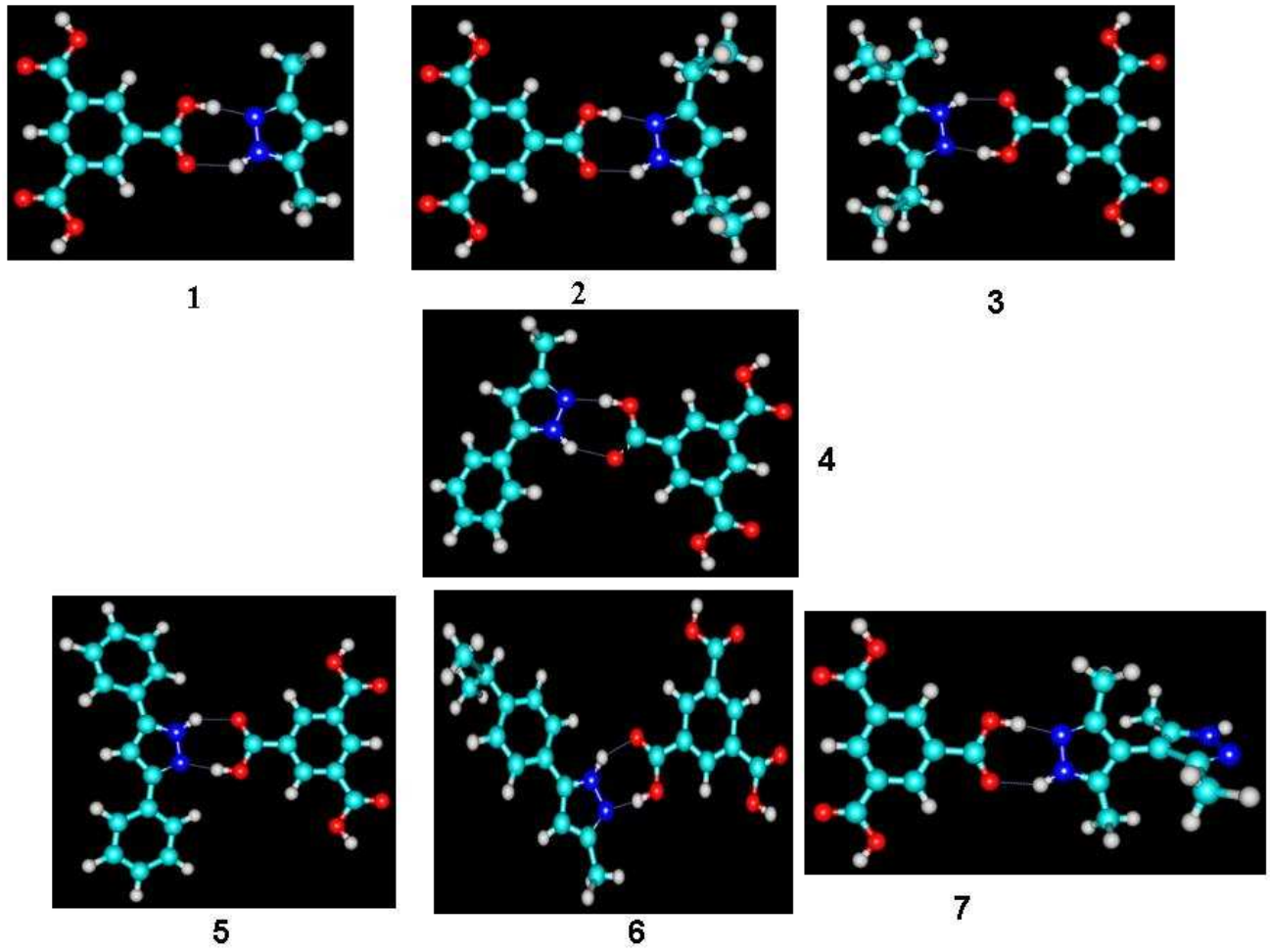

Fig. 11

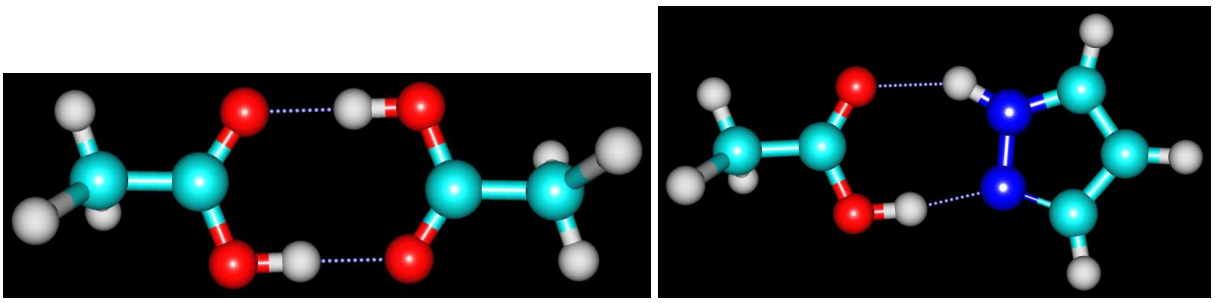

Fig. 12

Graphical Abstract

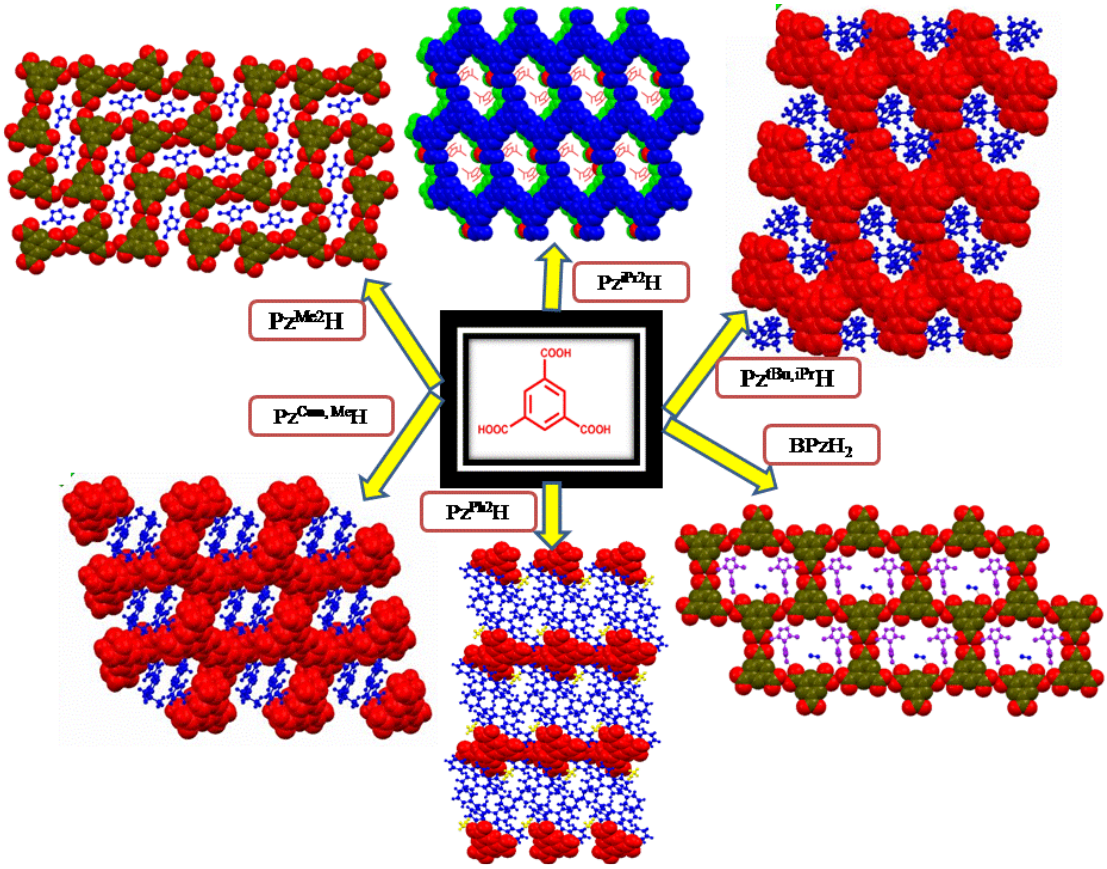

Reaction of benzene-1,3,5-tricarboxylic acid (H_3BTC) with various substituted pyrazoles viz., 3,5-dimethylpyrazole ($Pz^{Me2}H$), 3,5-diisopropylpyrazole ($Pz^{iPr2}H$), 3-tert-butyl-5-isopropylpyrazole ($Pz^{tBu,iPr}H$), 3-phenyl-5-methylpyrazole ($Pz^{Ph,Me}H$), 3-cumenyl-5-methylpyrazole ($Pz^{Cum,Me}H$), 3,5-diphenylpyrazole ($Pz^{Ph2}H$) and 3,3′,5,5′-tetramethyl-4,4′-bipyrazole (BPzH2) resulted in different host guest assembly. Theoretical calculations were used to calculate the interaction energy and their comparison with the experimental data obtained through thermo-gravimetric analysis. Energies of the various synthons were also calculated to correlate their stability and occurrence with the change in the substituents present on pyrazoles.